A Ni-Fe-Cu Center in a Bifunctional Carbon Monoxide Dehydrogenase/ Acetyl-CoA Synthase

Tzanko I. Doukov,[1] Tina M. Iverson,[1]* Javier Seravalli,[2] Stephen W. Ragsdale,[2] Catherine L. Drennan[1]†

A metallocofactor containing iron, sulfur, copper, and nickel has been discovered in the enzyme carbon monoxide dehydrogenase/acetyl-CoA (coenzyme A) synthase from *Moorella thermoacetica* (f. *Clostridium thermoaceticum*). Our structure at 2.2 angstrom resolution reveals that the cofactor responsible for the assembly of acetyl-CoA contains a [Fe_4S_4] cubane bridged to a copper-nickel binuclear site. The presence of these three metals together in one cluster was unanticipated and suggests a newly discovered role for copper in biology. The different active sites of this bifunctional enzyme complex are connected via a channel, 138 angstroms long, that provides a conduit for carbon monoxide generated at the C-cluster on one subunit to be incorporated into acetyl-CoA at the A-cluster on the other subunit.

Acetogenic bacteria such as *Moorella thermoacetica* (f. *Clostridium thermoaceticum*) can grow autotrophically on the greenhouse gas CO_2. These organisms use the Wood-Ljungdahl carbon fixation pathway to convert CO_2 to acetyl-CoA (*1, 2*). The bifunctional carbon monoxide dehydrogenase/acetyl-CoA synthase (CODH/ACS), which is responsible for reduction of CO_2 to CO and subsequent assembly of acetyl-CoA, is a key enzyme in this pathway. Methanogenic archaea also use CODH/ACS enzymes. In these organisms, however, CODH/ACS is used in the degradation of acetyl-CoA to form methane and CO_2. Because of their unusual metalloclusters, their use of biological organometallic reaction intermediates, and their role in reducing levels of the gaseous pollutants CO and CO_2 in our environment, CODH/ACS enzymes have been the subject of intense study (*1, 2*). Here we present the 2.2 Å resolution crystal structure of the most extensively characterized bifunctional CODH/ACS. [Coordinates have been deposited in the Brookhaven Protein Data Bank (accession code 1MJG).]

The *M. thermoacetica* enzyme is a 310-kD $\alpha_2\beta_2$ heterotetramer that catalyzes two different reactions. The C-cluster in the CODH subunit (β) generates CO from CO_2, while the A-cluster of the ACS subunit (α) combines the CO with CoA and a methyl group to form acetyl-CoA (Scheme 1). Remarkably, a channel appears to connect the enzyme active sites so that CO generated at the C-cluster is selectively incorporated into acetyl-CoA at the A-cluster (*3, 4*). The methyl group, which is incorporated into acetyl-CoA, is transferred to the A-cluster by a corrinoid iron-sulfur protein (CFeSP). Thus, the synthesis of acetyl-CoA at the A-cluster involves a methyl group transfer reaction, a carbonylation reaction, and synthesis of a high-energy thioester bond.

The mechanism by which acetyl-CoA is assembled at the A-cluster is controversial, as is the mechanism of CO_2 reduction at the C-cluster. Recently, a structure of the well-characterized *Rhodospirillum rubrum* CODH (*5*) and the structure of *Carboxydothermus hydrogenoformans* CODH (*6*) have become available. The x-ray analyses revealed that the C-cluster was not as expected from spectroscopic analyses. Instead of a [Fe_4S_4] cubane bridged to a mononuclear Ni site, the Ni is part of a Fe-[$NiFe_3S_4$] cluster. The A-cluster was also thought to be an [Fe_4S_4] cubane bridged to a mononuclear Ni site. However, the structural analysis presented here reveals that the A-cluster contains a [Fe_4S_4] cluster bridged to a binuclear site. Dispersive difference Fourier calculations suggest that the binuclear site contains one Cu and one Ni atom. Here, we address the structure and mechanism of the A-cluster, describe a putative CO channel, and address how the A-cluster may interact with substrates CO, CFeSP, and CoA.

Overall enzyme structure, channels, and protein-protein interactions. The structure of CODH/ACS from *M. thermoacetica* was solved by multiwavelength anomalous dispersion (MAD) techniques (Table 1). The structure of the 310-kD $\alpha_2\beta_2$ heterotetramer is shown in Fig. 1A. The overall shape of the molecule is similar to the electron microscopy reconstruction of *M. thermoacetica* CODH/ACS (*1*). The β_2 domains form the center of the complex. These domains are responsible for $CO_2 \leftrightarrow$ CO chemistry and contain the B-, C-, and D-clusters. The β_2 subunits of CODH closely resemble the structures of *R. rubrum* and *C. hydrogenoformans* CODH (*5, 6*) with root-mean-square (RMS) deviations of 1.0 Å (610 α carbons) and 0.8 Å (614 α carbons), respectively. On each end of the complex is an α subunit containing the A-cluster responsible for acetyl-CoA synthesis. The distance between the C- and the A-clusters is about 67 Å. With this long distance, direct electron transfer between these clusters is unlikely to occur at a rate sufficient to explain the reductive activation of the A-cluster. Although the direct source of electrons for the reductive activation of the A-cluster is unknown, ferredoxin is a likely candidate. Ferredoxin stimulates the exchange of CO with $CH_3{}^{14}COCoA$ (*7*) and cross-links to the α subunit of ACS (*8*). The crystal structure reveals that the [Fe_4S_4] moiety of the A-cluster is very close to the surface of the enzyme, where interaction with an electron transfer protein would be possible.

The long distance between the C- and A-clusters is interesting given the evidence for a CO channel between these sites (*3, 4*). Using the program CAVENV (*9*), we have identified cavities connecting CODH and ACS, consistent with the biochemical data. Figure 1B shows that there is indeed a long hydrophobic cavity through the middle of the protein complex that runs about 138 Å from A-cluster to A-cluster with branches to each C-cluster. Although the two C-clusters are about the same distance (~67 Å) from either A-cluster, Fig. 1B shows that the most direct route would be from clusters C to A and C′ to A′. Enzymes with multiple active sites typically use channels to transport reactive intermediates (*10*). Because CO cannot be considered a reactive intermediate, the roles of this channel must be different and could include synchronizing cluster activities, increasing the local concentration of CO at the A-cluster, directing CO to a productive rather than inhibitory binding site on the A-cluster, and preventing cellular CO toxicity. It has been

CODH Subunit:

C-cluster $CO_2 + 2H^+ + 2e^- \longleftrightarrow CO + H_2O$

B- and D-clusters Electron transfer

ACS Subunit:

A-cluster CH_3-Co(III)-CFeSP + CO + HSCoA $\longleftrightarrow$ $CH_3-\overset{\overset{O}{\|}}{C}-SCoA$ + Co(I)-CFeSP + H^+

Scheme 1.

[1]Department of Chemistry, Massachusetts Institute of Technology, Cambridge, MA 02139, USA. [2]Department of Biochemistry, Beadle Center, University of Nebraska, Lincoln, NE 68588, USA.

*Present address: Division of Biomedical Sciences, MPC, Imperial College of Science, Technology and Medicine, London SW7 2AZ, UK.

†To whom correspondence should be addressed. E-mail: cdrennan@mit.edu

suggested that the hydrophobic channel for molecular hydrogen in the Ni-Fe hydrogenase enzyme can be thought of as a gas reservoir, and that all gas-metabolizing enzymes will have hydrophobic channels or cavities for gas storage and active site access (*11*). Our findings are certainly consistent with this idea. It is interesting that all CODH/ACS active sites are connected, because one channel between each set of active sites should suffice. The long distance between the C- and A-clusters can be rationalized in terms of preventing electron transfer between the clusters. The reduction of CO_2 at the C-cluster requires two electrons to generate the CO substrate for the A-cluster (Scheme 1). If electrons were transferred from the A- to the C-cluster, the A-cluster would be inactivated.

The α subunit of ACS is composed of three domains (Fig. 1C). The first domain comprises a helical region at the NH_2-terminus of a Rossmann (six-stranded α/β) fold. This domain resembles the helical region and one of the Rossmann domains of the β_2 subunits and could have resulted from gene duplication. The second and third domains are α + β folds that do not align well with known structural motifs in the DALI structural database (*12*). A dominant feature of the α subunit is the large cavity between the three domains (Fig. 1C). The presence of Trp^{418} and six Arg residues in this region suggests that the cavity may represent the binding site for CoA. Trp^{418} exhibits a change in fluorescence upon CoA binding (*13*), and the Arg-specific reagent phenylglyoxal inhibits binding of CoA (*7*). CoA can be modeled into the cavity so that it can access the A-cluster with only a slight adjustment of protein side chains. In contrast, the modeling of a corrinoid cofactor into the cavity suggests that the methyl transfer reaction cannot occur without further protein rearrangements. Although the presence of a Ni-methyl intermediate has not been directly demonstrated, the transfer of a methyl group from the corrinoid to the A-cluster is proposed to occur by an S_N2 nucleophilic substitution mechanism with the Ni of the A-cluster acting as the nucleophile (*14*). For such a transfer to occur, the corrinoid cofactor would have to be positioned directly above the Ni. In the ACS structure, this site is occupied by atoms of domain 1 (Fig. 1C). However, a subtle shift of domain 3 with respect to domain 1 would allow the corrinoid cofactor to access this site. Such a domain shift seems possible because all the ligands to the A-cluster are from one domain (domain 3), the number of hydrogen-bonding contacts and buried surface area between the domains is minimal, and the domains are connected by long flexible loops (Fig. 1C). The presence of the A-cluster at a domain interface explains how the enzyme solves the problem of providing access of the large protein-bound corrinoid cofactor while still protecting the active site during catalysis.

Identity of metals in the A-cluster. Electron density maps suggest that the A-cluster contains a binuclear site coordinated to a four-metal cubane ($[Fe_4S_4]$-X-M_a-X-M_b). To verify that the four-metal cubane is an $[Fe_4S_4]$ cluster, and to identify the metals M_a and M_b, we performed a series of multiwavelength dispersion experiments (data in Table 1). These calculations identify the four-metal cluster as a $[Fe_4S_4]$ cubane, the M_a site as Cu, and the M_b site as Ni (Fig. 2A). Because zinc has also been found in the enzyme in variable amounts (*15*), dispersive electron density maps have been calculated with data collected near the Zn peak wavelength (1.28233 Å) to look for the presence of

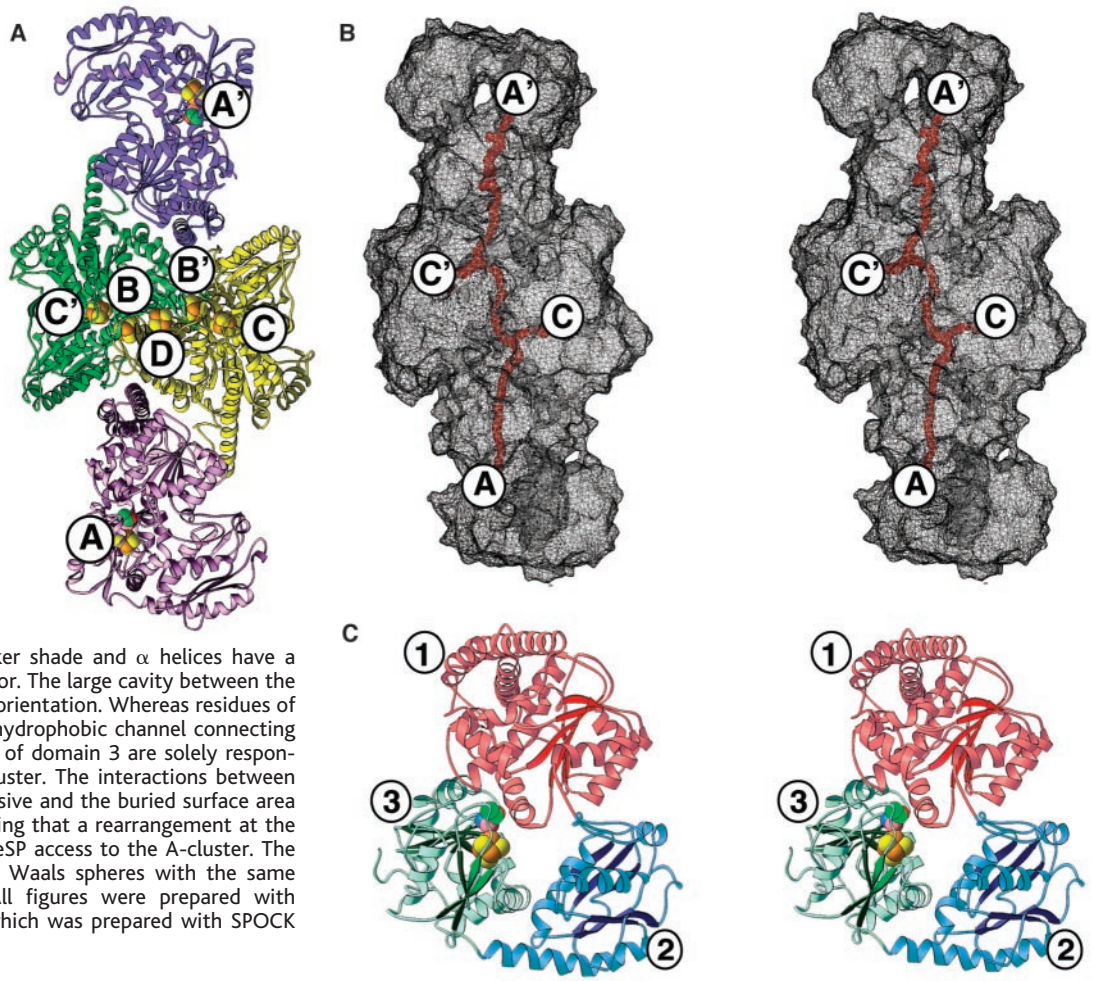

Fig. 1. (**A**) Structure of CODH/ACS from *M. thermoacetica*. The α domains are light and dark purple; the β domains are green and yellow. The metalloclusters A, B, C, and D are shown as van der Waals spheres with the following color scheme: yellow, S; orange, Fe; pink sphere, Cu; blue sphere, Ni; green, C; blue, N; red, O. The distance between A- and C-clusters is about 67 Å. (**B**) Stereoview of putative channel for CO as calculated by program CAVENV with a sphere size of 3 Å. The orientation of this figure is about the same as in (A). (**C**) Stereoview of the α subunit. The three domains are labeled 1 (residues 1 to 314, red), 2 (residues 315 to 494, blue), and 3 (residues 495 to 729, green) based on their order in the primary sequence. β strands have a darker shade and α helices have a lighter shade of the domain color. The large cavity between the three domains is visible in this orientation. Whereas residues of domain 1 serve to create the hydrophobic channel connecting the C- and A-clusters, residues of domain 3 are solely responsible for coordinating the A-cluster. The interactions between domains 1 and 3 are not extensive and the buried surface area is not large (1600 $Å^2$), suggesting that a rearrangement at the interface could provide the CFeSP access to the A-cluster. The A-cluster is shown as van der Waals spheres with the same coloring scheme as in (A). All figures were prepared with Ribbons (*42*), except for (B), which was prepared with SPOCK (*43*).

Zn in the structure. No peaks above the noise level are observed, ruling out a high-occupancy Zn site. It is not possible, however, to rule out the presence of Zn at partial occupancies in the M_a site or elsewhere on the protein.

The presence of a $[Fe_4S_4]$-X-Cu-X-Ni metallocenter is surprising, given that there are no other examples of Fe-S-Cu-Ni together in one cofactor. Although Cu content has not been reported in the literature for CODH/ACS, metal analysis has revealed as much as 0.68 mol of Cu per mol of αβ heterodimer (Table 2). The substoichiometric amounts of Cu in the enzyme are consistent with the reports of A-cluster heterogeneity (*2*). The NiFeC electron paramagnetic resonance (EPR) signal used as an indication of the percentage of functional A-clusters in the enzyme is typically 0.3 to 0.4 spin and never reaches the expected 1 spin per αβ heterodimer. We find that the amount of Cu in the enzyme does correlate with a higher spin quantitation (Table 2). It also correlates with a higher A-cluster activity but not with a higher C-cluster activity (Table 2). This is consistent with Cu being a functional component of the A-cluster but not a functional component of the C-cluster. Because samples with 0.68 mol of Cu have only 0.28 spin per αβ heterodimer, Cu stoichiometry alone cannot explain all the A-cluster heterogeneity. Some of the heterogeneity could be because all active sites are connected (Fig. 1B). In addition to the CO channel linking all four active sites, the B- and D-clusters provide a path for electrons to flow between the two C-clusters (Fig. 1A). This connectivity could limit the percentage of clusters in one form at any time.

Table 1. Crystallographic analysis. *M. thermoacetica* (f. *C. thermoaceticum* strain ATCC 39073) CODH/ACS was purified under strictly anaerobic conditions as described (*15, 32*). Crystals were grown by standard sitting drop vapor diffusion at room temperature in a Coy anaerobic chamber. The sitting drops consisted of 5 μl of protein solution [CODH/ACS at 40 to 60 mg/ml in 50 mM tris (pH 7.6)] mixed with 7.5 μl of reservoir solution [8% polyethylene glycol MME 5000, 20% glycerol, 200 mM calcium acetate, 100 mM Pipes (pH 6.5), and 2 mM dithioerythritol]. Crystals belong to space group P1, with two $\alpha_2\beta_2$ heterotetramers per asymmetric unit (a = 99.85, b = 136.80, c = 141.06 Å, α = 101.22, β = 109.08, γ = 104.08°). For data collection, crystals were flash-cooled in liquid nitrogen with 20% glycerol as a cryoprotectant. Data were collected at the Advanced Light Source (ALS) beamline 5.0.2 equipped with an charge-coupled device detector (Area Detector Systems Corp.) and processed and scaled with Denzo and Scalepack (*33*). MAD data were collected by an inverse beam method, and the Fe sites were found by SHELXD (*34*) and refined in CNS (*35*). With data collected at wavelengths 1.2000, 1.7389, and 1.7422 Å, the final overall figure of merit was 0.61 to 3.8 Å resolution. A molecular replacement solution was also obtained using a second crystal form of CODH/ACS collected at 0.88 Å wavelength (space group P1 with cell dimensions: a = 99.45, b = 139.84, c = 149.04 Å, α = 104.73, β = 105.76, γ = 106.15°) and the coordinates for CODH (1JQK) in EPMR (*36*). The quality of the electron density maps improved when the experimental phases were combined with molecular replacement phases and subjected to multicrystal averaging and fourfold NCS-averaged with programs DMMULTI (*37*) and DM (*38*). Iterative rounds of model building in Xtalview (*39*) and O (*40*), refinement in CNS (*35*), phase combination and extension in DM, and averaging resulted in the 2.2 Å resolution model described below. A bulk solvent correction, with no σ data cutoff, NCS restraints, the maximum-likelihood target function, and cartesian molecular dynamics were used in the CNS refinement; 14,965 reflections were used to calculate R_{free}. The refined structure contains residues 2 to 729 of the α subunit and 2 to 674 of the β subunit in both $\alpha_2\beta_2$ complexes in the asymmetric unit (asu). Regions present in the model that have high B-factors (70 to 90 Å^2) and/or poor quality electron density include 313 to 317 in α and 533 to 542 in β. The present model exhibits good geometry with 96.8% of the residues residing in allowed regions of the Ramachandran plot as calculated by PROCHECK (*41*).

Data statistics

Wavelength (Å)	Resolution range (Å)	Unique reflections	Total reflections	Completeness (%)	R_{sym}
0.88000	100 to 3.0	132,821	242,015	96.5 (95.3)	8.8 (30.6)
1.20000	50 to 2.2	313,013	1,031,478	95.1 (91.3)	9.3 (39.0)
1.28233*	50 to 2.5	437,662	799,644	95.7 (92.0)	5.8 (25.0)
1.38000*	50 to 2.5	422,835	791,235	92.5 (62.6)	4.6 (18.1)
1.48662*	50 to 2.4	482,097	1,789,716	94.2 (75.6)	6.8 (30.3)
1.7389*	50 to 3.3	191,198	390,044	94.8 (81.0)	4.0 (8.4)
1.7422*	50 to 3.3	190,212	404,417	96.1 (93.0)	3.8 (7.2)

Refinement statistics

Nonhydrogen atoms in asymmetric unit	43,452 (protein and cofactor)
Water molecules in asymmetric unit	1,209
Resolution range (Å)	20 to 2.2
Number of reflections (test set)	301,055 (14,965)
R_{cryst} (%)	22.0
R_{free} (%)	25.2
RMS deviations of protein from ideal geometry	
Bonds (Å)	0.0096
Angles (°)	1.4454
Average B (Å^2) for molecules 1, 2, 3, and 4 in the asu	
Protein α	35.0 (1), 34.1 (2), 75.7 (3), 58.5 (4)
Protein β	28.1 (1), 25.8 (2), 32.7 (3), 36.4 (4)
A-cluster	20.2 (1), 21.1 (2), 80.5 (3), 47.3 (4)

*For these data sets, Friedel pairs were not merged during data processing. $R_{sym} = [\Sigma_{hkl}\Sigma_i |I_i(hkl) - \langle I(hkl)\rangle|]/\Sigma_{hkl}\Sigma_i I_i(hkl)$ for n independent reflections and i observations of a given reflection. $\langle I(hkl)\rangle$ is the average intensity of the i observation. Values for data in the highest resolution bin are listed in parentheses.

Description of the A-cluster. Models of the A-cluster are shown in Fig. 2, B and D. The $[Fe_4S_4]$ component of the A-cluster is a typical $[Fe_4S_4]$ center coordinated by four Cys residues—Cys^{506}, Cys^{509}, Cys^{518}, and Cys^{528}—in agreement with EPR, Mössbauer, and electron nuclear double resonance spectroscopic data (*2, 16*). One of the Cys ligands to the $[Fe_4S_4]$ center, Cys^{509}, bridges between the $[Fe_4S_4]$ cluster and the binuclear site. This type of assembly is reminiscent of the Fe-only hydrogenase structure, which contains a $[Fe_4S_4]$ bridged by a Cys residue to a binuclear Fe site (*17, 18*). In ACS, the metal closest to the $[Fe_4S_4]$ cluster is Cu. The coordination geometry at the Cu is distorted tetrahedral. In addition to being coordinated by Cys^{509}, Cu is connected to the Ni via two Cys side chains, Cys^{595} and Cys^{597} (Fig. 2, B and D). The fourth ligand is a nonprotein ligand of unknown composition, which is discussed below. The Ni atom has square planar geometry and is coordinated by the side chains of Cys^{595} and Cys^{597} and by two backbone N atoms of Gly^{596} and Cys^{597} (Fig. 2, B and D). Extended x-ray absorption fine structure data (*19*) suggest that the Ni has square planar geometry with two S donors at 2.19 Å and two N/O donors at 1.89 Å, in

Table 2. Cu metal analysis and NiFeC EPR spin quantitation of two CODH/ACS protein samples. Metal analyses were performed by plasma emission spectroscopy. X-band EPR spectra were recorded in a Bruker ESP300e spectrometer equipped with a Hewlett-Packard microwave frequency counter (model 5253B), a Bruker Gaussmeter (model ER 035), and an Oxford ITC4 temperature controller. Activity assays were performed as described (*15*).

	Sample 1	Sample 2
Fe (14 mol/αβ expected)	11.27	14.36
Ni (2 mol/αβ expected)	1.64	2.25
Cu	0.41	0.68
Zn	0.45	0.47
C-cluster activity (CO oxidation)	500	485
A-cluster activity (acetyl-CoA/CO exchange)	200	250
NiFeC (1 spin/αβ expected)	0.18	0.28

agreement with the x-ray structure. All residues contacting the A-cluster are strictly conserved in all known sequences of ACS enzymes.

In all four α subunits in the asymmetric unit, there is electron density for a nonprotein ligand on the Cu (Fig. 2E). Refinement of a nonlinear three-atom molecule, such as a metal-acetyl species, results in no positive or negative difference density, indicating that this is the correct size of the unknown ligand. The presence of a three-atom molecule on Cu is intriguing given that a three-atom molecule, metal-acetyl, is a known reaction intermediate. When CoA is absent from the reaction mixture, acetate forms via hydrolysis of the metal-acetyl intermediate (*7, 20*). A stable acetyl-ACS intermediate is also implicated when ACS reacts with acetyl-CoA (*2, 16*). Although acetate itself is not a good fit to this electron density, the high concentration of acetate in the crystallization conditions (100 to 200 mM) may have allowed us to capture the structure of a metal-acetyl intermediate enzyme form. It is also possible that the acetylated form of CODH/ACS has been selectively crystallized. Inspection of the domain 1–domain 3 interface suggests that an acetyl moiety bound to Cu could serve as a peg in a hole, restricting the movement of domain 3 with respect to domain 1. Thus, the fraction of enzyme that is acetylated could be less conformationally flexible and crystallize more readily. Another possibility is that a bent CO molecule oriented in two discrete conformations could give rise to this electron density shape. However, infrared spectroscopy results indicate a single mode of CO binding to the A-cluster (*21*). Although it is not possible to definitively identify this ligand, the possibility of a Cu-acetyl or Cu-CO species is intriguing and is consistent with the mechanistic proposal described below.

Mechanistic significance of the structure. Ni coordination by protein backbone N atoms was unexpected. Although there are several examples of this type of coordination for Ni and Cu with peptides (*22*), it has not been observed in structures of other Ni-dependent enzymes. In fact, the coordination of metals by backbone N atoms in proteins is very rare, with serum albumin (*22*) and nitrile hydratase being the only well-characterized examples (*23, 24*). Interestingly, both nitrile hydratase and ACS use a Cys-X-Cys motif (Fig. 2B) in which the two Cys side chains and two backbone N atoms coordinate the metal with square planar geometry. In nitrile hydratase, the metal is Fe and the pseudo-ring system created by the protein has been compared with a heme (*23*). For ACS, the pseudo-ring system created by the protein for Ni is reminiscent of the Ni corphinoid ring system of methyl–coenzyme M reductase (MCR) (*25*).

The close resemblance between the Ni corphinoid of MCR and the Ni site in ACS is intriguing, because the chemistry performed by Ni in both enzymes may be similar. For both, Ni has been proposed to act as a nucleophile attacking the methyl group of a substrate and forming a methyl-Ni intermediate (*14, 26*). In MCR the methyl group undergoes protonolysis to form methane, whereas in ACS methyl migration (carbonyl insertion) occurs to form an acetyl-enzyme

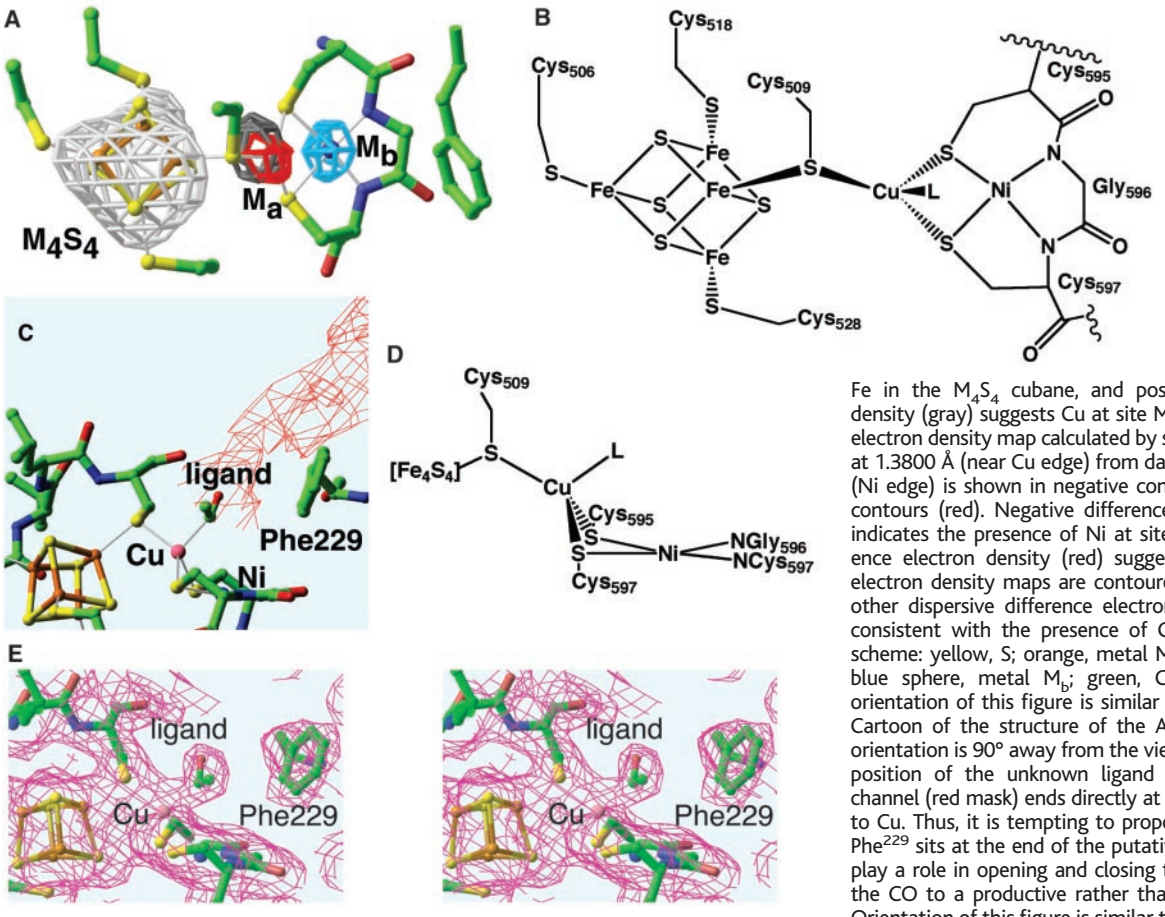

Fig. 2. (**A**) Identification of metals in the A-cluster. A dispersive difference electron density map calculated by subtracting data collected at 1.3800 Å (Cu edge) from data collected at 1.7422 Å (Fe edge) is shown in negative contours (white) and positive contours (gray). Negative difference electron density (white) indicates the presence of Fe in the M_4S_4 cubane, and positive difference electron density (gray) suggests Cu at site M_a. A dispersive difference electron density map calculated by subtracting data collected at 1.3800 Å (near Cu edge) from data collected at 1.48662 Å (Ni edge) is shown in negative contours (blue) and positive contours (red). Negative difference electron density (blue) indicates the presence of Ni at site M_b, and positive difference electron density (red) suggests Cu at site M_a. Both electron density maps are contoured at 6σ. Note that four other dispersive difference electron density maps are also consistent with the presence of Cu at the M_a site. Color scheme: yellow, S; orange, metal M; pink sphere, metal M_a; blue sphere, metal M_b; green, C; blue, N; red, O. The orientation of this figure is similar to that shown in (B). (**B**) Cartoon of the structure of the A-cluster (top view). This orientation is 90° away from the view in (D). L represents the position of the unknown ligand (see text). (**C**) The CO channel (red mask) ends directly at the position of the ligand to Cu. Thus, it is tempting to propose that CO binds to Cu. Phe^{229} sits at the end of the putative CO channel and could play a role in opening and closing the tunnel or in directing the CO to a productive rather than inhibitory binding site. Orientation of this figure is similar to that in (D). (**D**) Cartoon of the structure of the A-cluster (side view). This orientation is 90° away from the view in (B). L represents the position of the unknown ligand (see text). (**E**) Stereoview of an omit electron density map (pink) of the A-cluster with an acetyl group modeled into the extra density at the Cu. Although the identity of this ligand to Cu is unknown, a three-atom ligand such as an acetyl moiety is the correct size. Three water molecules cannot explain the electron density either, because they would have to be placed too close together (<2.0 Å apart). Phe^{229} makes van der Waals contacts with the unknown ligand. Orientation of this figure is similar to that in (D). Color scheme is the same as in Fig. 1A.

intermediate. In the latter reaction, model chemistry predicts that the CO and methyl are at least transiently on the same metal. However, the x-ray structure shows that the Cys-X-Cys motif restricts the only open coordination sites to be trans to each other (Fig. 2D). It is unlikely that a protein rearrangement could result in an open cis-coordination site, because the Cys ligands are held in place via backbone interactions with the Ni and via side chain interactions with the Cu. Therefore, for the CO and methyl group to react, we propose a binuclear mechanism involving both Cu and Ni in catalysis. Although several different mechanisms can be written, one possible scenario is given in Fig. 3 and described below. We suggest that Ni binds the methyl group in agreement with several pieces of biochemical data (*27*) and reminiscent of the proposed methyl-Ni intermediate of MCR. Fourier transform infrared spectroscopic studies have demonstrated that CO is terminally bound to one of the metals in the A-cluster (*21*). We suggest that CO is terminally bound to Cu(I). Cu(I) forms stable complexes with CO in model systems and in some metalloenzymes (*28*). The putative CO channel, which connects the Ni of the C-cluster with the Cu of the A-cluster, is also consistent with this proposed CO binding site (Fig. 2C). In the binuclear mechanism, a CO molecule bound to Cu would be ideally positioned to react with a Ni-methyl moiety to form an acetyl-Cu intermediate. There also is literature precedent for formation of an acetyl-Cu species via reaction of Cu(I)-CO with a methyl radical (*29*). Modeling indicates that a CO molecule on Cu and a methyl group on Ni would be at an appropriate angle and at an appropriate distance (about 1.6 to 1.8 Å apart) to react with each other (see Fig. 3). The oxidation state of the A-cluster during catalysis is controversial, and an x-ray structure cannot resolve this issue. However, the proposal that a redox-active Cys pair called the D-site (*27*) is involved in catalysis appears unlikely, because all Cys in the active site are intimately involved in the cluster assembly.

Given that CODH/ACS must perform a series of molecular juggling acts during catalysis, multiple conformations of the enzyme must be possible. The conformation of the enzyme captured in the x-ray structure appears to be closed. Cavity calculations indicate that, although the A-cluster is very close to the surface of the protein, the best route for CO to the A-cluster is from the C-cluster via the putative channel (Fig. 2C). CO can also inhibit acetyl-CoA synthesis (*30*) by interfering with methylation (*31*). The structure suggests that Phe^{229} could play the role of a gatekeeper, directing the CO to the Cu and protecting the Ni. Thus, CO entering the active site via the channel would bind productively to Cu, whereas under high CO concentrations, solution CO could bind both Cu and Ni and serve as both inhibitor and substrate. For the methyl transfer between the corrinoid cofactor and the Ni of the A-cluster (Fig. 3), an open corrinoid conformation would be required, perhaps created by the sliding of domain 3 with respect to domain 1 (Fig. 1C). In contrast, an A-cluster that is protected from solvent during acetyl intermediate formation would help to explain the incorporation of CO generated at the C-cluster, rather than solution CO, into acetyl-CoA (*3, 4*). Once the acetyl intermediate is formed, the enzyme would need to adopt an open conformation to allow CoA access (see Fig. 3). After binding, HSCoA is deprotonated and acetylated. There is no obvious conserved residue near the active site that could act as a base to deprotonate HSCoA, suggesting that a transient interaction between CoA and one of the metals of the A-cluster could facilitate this reaction. Docking of CoA into the active site suggests that it would be positioned near Cu with an appropriate geometry to react with a Cu-bound acetyl moiety.

We have described the structure of the well-characterized CODH/ACS from the model acetogen *M. thermoacetica*. In the biological equivalent of the Monsanto industrial process, CODH/ACS condenses CO, formed by CODH, with a methyl group and CoA to form acetyl-CoA. The structure of the catalyst in the ACS reaction has now been identified as an $[Fe_4S_4]$ cubane bridged to a Cu-Ni binuclear center. The organization of the metals in the A-cluster suggests that Cu and Ni are involved in a binuclear catalytic mechanism. We also have defined a channel 138 Å long that sequesters CO, preventing its release into solution. This channel prevents CO toxicity to the microbe's host (including ruminants and humans) and retains this energy-rich compound at the site of reaction.

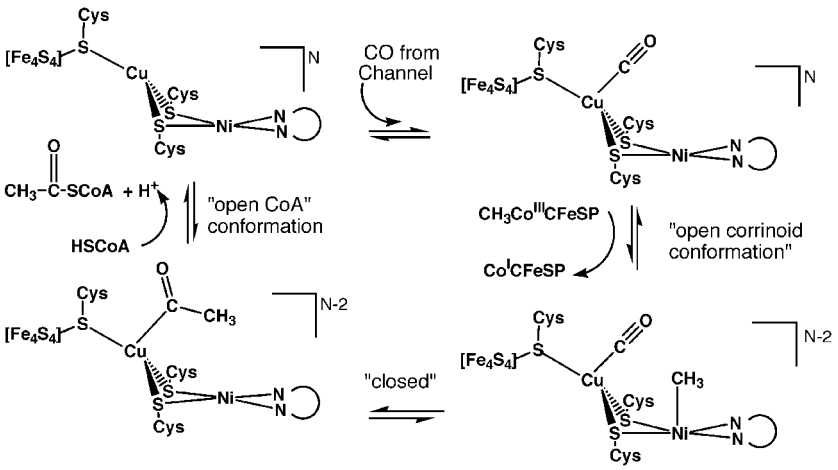

Fig. 3. Simplistic mechanistic proposal for acetyl-CoA synthase activity. Although experimental data indicate that the reaction of an acetyl-metal intermediate with CoA is the last step in the mechanism (*7, 20*), the data do not distinguish between CO binding and methylation as the first step. In this scenario, we propose that CO generated from CO_2 at the C-cluster travels through the putative channel and binds to Cu. Ni has been proposed to act as a nucleophile attacking the methyl group of protein-bound methylcob(III)amide, resulting in cob(I)amide and a methylated Ni species (*14*). The reaction of CO and methyl group could proceed through an alkyl migration yielding an acetyl-metal–bound intermediate. In the final step, HSCoA is deprotonated and acetylated. The oxidation states of metals during catalysis are highly controversial (*2, 31*) and cannot be resolved here. However, the presence of three Cu thiolate ligands suggests that Cu is likely to be in the Cu(I) oxidation state throughout catalysis. The coordination of Ni by two thiolates and two deprotonated peptide nitrogens should favor higher oxidation states of Ni: Ni(II) with no axial ligands and Ni(III) when an axial ligand is bound (*44*). The presence of the $[Fe_4S_4]$ moiety of the A-cluster close to the surface of the enzyme suggests that oxidation states including all ferrous could be considered for this cubane (*45*).

References and Notes

1. S. W. Ragsdale, M. Kumar, *Chem. Rev.* **96**, 2515 (1996).
2. P. A. Lindahl, *Biochemistry* **41**, 2097 (2002).
3. J. Seravalli, S. W. Ragsdale, *Biochemistry* **39**, 1274 (2000).
4. E. L. Maynard, P. A. Lindahl, *J. Am. Chem. Soc.* **121**, 9221 (1999).
5. C. L. Drennan, J. Heo, M. D. Sintchak, E. Schreiter, P. W. Ludden, *Proc. Natl. Acad. Sci. U.S.A.* **98**, 11973 (2001).
6. H. Dobbek, V. Svetlitchnyi, L. Gremer, R. Huber, O. Meyer, *Science* **293**, 1281 (2001).
7. S. W. Ragsdale, H. G. Wood, *J. Biol. Chem.* **260**, 3970 (1985).
8. T. Shanmugasundaram, H. G. Wood, *J. Biol. Chem.* **267**, 897 (1992).
9. A. Volbeda, *Ecoles Phys. Chim. Vivant* **1**, 47 (1999).
10. J. B. Thoden, H. M. Holden, G. Wesenberg, F. M. Raushel, I. Rayment, *Biochemistry* **36**, 6305 (1997).

11. Y. Montet *et al*., *Nature Struct. Biol.* **4**, 523 (1997).
12. L. Holm, C. Sander, *Proteins* **19**, 165 (1994).
13. T. Shanmugasundaram, G. K. Kumar, H. G. Wood, *Biochemistry* **27**, 6499 (1988).
14. S. Menon, S. W. Ragsdale, *J. Biol. Chem.* **274**, 11513 (1999).
15. S. W. Ragsdale, J. E. Clark, L. G. Ljungdahl, L. L. Lundie, H. L. Drake, *J. Biol. Chem.* **258**, 2364 (1983).
16. S. W. Ragsdale, in *Enzyme-Catalyzed Electron and Radical Transfer*, A. Holzenburg, N. Scrutton, Eds. (Plenum, New York, 2000), vol. 35, pp. 487–518.
17. J. W. Peters, W. N. Lanzilotta, B. J. Lemon, L. C. Seefeldt, *Science* **282**, 1853 (1998).
18. Y. Nicolet, C. Piras, P. Legrand, C. E. Hatchikian, J. C. Fontecilla-Camps, *Structure* **7**, 13 (1999).
19. W. K. Russell, C. M. V. Stalhandske, J. Q. Xia, R. A. Scott, P. A. Lindahl, *J. Am. Chem. Soc.* **120**, 7502 (1998).
20. S.-I. Hu, H. L. Drake, H. G. Wood, *J. Bacteriol.* **149**, 440 (1982).
21. M. Kumar, S. W. Ragsdale, *J. Am. Chem. Soc.* **114**, 8713 (1992).
22. C. Harford, B. Sarkar, *Acc. Chem. Res.* **30**, 123 (1997).
23. W. Huang *et al*., *Structure* **5**, 691 (1997).
24. S. Nagashima *et al*., *Nature Struct. Biol.* **5**, 347 (1998).
25. U. Ermler, W. Grabarse, S. Shima, M. Goubeaud, R. K. Thauer, *Science* **278**, 1457 (1997).
26. R. K. Thauer, *Microbiology UK* **144**, 2377 (1998).
27. D. P. Barondeau, P. A. Lindahl, *J. Am. Chem. Soc.* **119**, 3959 (1997).
28. S. Jaron, N. J. Blackburn, *Biochemistry* **38**, 15086 (1999).
29. A. Szulc, D. Meyerstein, H. Cohen, *Inorg. Chim. Acta* **270**, 440 (1998).
30. E. L. Maynard, C. Sewell, P. A. Lindahl, *J. Am. Chem. Soc.* **123**, 4697 (2001).
31. J. Seravalli, M. Kumar, S. W. Ragsdale, *Biochemistry* **41**, 1807 (2002).
32. J. R. Andreese, A. Schaupp, C. Neuraute, A. Brown, L. G. Ljungdahl, *J. Bacteriol.* **114**, 743 (1973).
33. Z. Otwinowski, W. Minor, *Methods Enzymol.* **276**, 307 (1997).
34. I. Uson, G. M. Sheldrick, *Curr. Opin. Struct. Biol.* **9**, 643 (1999).
35. A. T. Brünger *et al*., *Acta Crystallogr.* **D54**, 905 (1998).
36. C. R. Kissinger, D. K. Gehlhaar, D. B. Fogel, *Acta Crystallogr.* **D55**, 484 (1999).
37. K. Cowtan, *Joint CCP4 and ESF-EACBM Newsletter on Protein Crystallography* **31**, 34 (1994).
38. K. D. Cowtan, K. Y. Zhang, *Prog. Biophys. Mol. Biol.* **72**, 245 (1999).
39. D. E. McRee, *J. Struct. Biol.* **125**, 156 (1999).
40. T. A. Jones, J.-Y. Zou, S. W. Cowen, M. Kjeldgaard, *Acta Crystallogr.* **A47**, 110 (1991).
41. R. A. Laskowski, M. W. McArthur, D. S. Moss, J. M. Thornton, *J. Appl. Crystallogr.* **26**, 283 (1993).
42. M. Carson, *Methods Enzymol.* **277**, 493 (1997).
43. J. A. Christopher, thesis, Texas A&M University (1998).
44. M. L. Youngblood, D. W. Margerum, *Inorg. Chem.* **19**, 3068 (1980).
45. P. Strop *et al*., *Biochemistry* **40**, 651 (2001).
46. We thank T. Earnest and G. McDermott at Advanced Light Source (ALS) for help with data collection. Support has been provided by the Templeton Foundation (C.L.D.) and National Institutes of Health grant R01-GM39451 (S.W.R.). The data collection facilities at ALS are funded by the U.S. Department of Energy, Office of Basic Energy Sciences.

8 July 2002; accepted 3 September 2002

Shadows Cast by Retinal Blood Vessels Mapped in Primary Visual Cortex

Daniel L. Adams* and Jonathan C. Horton

The mammalian eye is a remarkable optical device, but its design is not perfect. The blood vessels that supply the inner retina are located in front of the photoreceptor layer, blocking access to light. Their shadows create a pattern of blindness in the field of vision that corresponds precisely to the location of the largest vessels in the eye. We show here that in squirrel monkeys, focal deprivation by blood vessels leads to rewiring of the eye's geniculocortical projections, imprinting an image of the retinal vascular tree onto the primary visual cortex. This process illustrates vividly that local imbalances in neuronal activity can influence column formation during normal development.

In many higher species, the geniculate afferents serving right and left eyes are segregated in the brain in layer 4 of primary (striate, V1) visual cortex into a mosaic of interdigitated inputs called ocular dominance columns (*1*). The formation of these columns has been scrutinized in the hope of elucidating the processes that guide the development of the cerebral cortex (*2*). Some experiments show an essential role for neuronal activity, because infusion of tetrodotoxin into both eyes seems to prevent the emergence of ocular dominance columns (*3*). According to this idea, the correlated discharge of neighboring ganglion cells, perhaps generated by spontaneous waves of retinal activity (*4*, *5*), induces local cortical imbalances in the density of geniculate afferents driven by each eye. These small imbalances may be amplified by competitive synaptic interactions between geniculocortical afferents to generate a mature system of ocular dominance columns (*6*–*9*).

Doubt has been cast on this explanation for column development by recent experiments showing that ocular dominance columns appear in ferrets despite early bilateral enucleation (*10*). This finding suggests that column formation is ordained by intrinsic molecular cues, and not by patterns of neuronal activity. Although neuronal activity has a disputed role in column induction, it certainly can influence column morphology at a later stage in development. Raising a newborn animal with monocular eyelid suture, to mimic congenital cataract, causes shrinkage of the deprived eye's columns and expansion of the normal eye's columns (*11*–*14*). Here, an imbalance in neuronal activity has a profound influence on the shape and size of the ocular dominance columns. The relevance of these experiments, however, can be questioned on the grounds that suture of the eyelids is an artificial manipulation, creating an extreme imbalance in the stimulation of each retina. It has not been shown that under natural circumstances, competition between the two eyes has an important influence on the appearance of the ocular dominance columns.

Cortical representation of retinal vessels. We now show that visual deprivation occurs routinely in normal primates, affecting ocular dominance patterns. Helmholtz discovered while plotting his blind spot that he could discern the proximal stumps of large blood vessels emerging from the optic disc (*15*). With refinement of perimetric techniques, subsequent investigators have plotted these so-called angioscotomas over wide portions of the visual field (*16*, *17*). The hemoglobin in red blood cells absorbs light, casting a shadow from blood vessels in the inner retina onto photoreceptors located underneath. We have found a representation of angioscotomas in striate cortex of the squirrel monkey (*Saimiri sciureus*).

The squirrel monkey was reported originally to lack ocular dominance columns (*18*, *19*). They are present, in fact, but often appear poorly developed and irregular (*20*). To examine their pattern more closely, we enucleated one eye and stained striate cortex for the mitochondrial enzyme cytochrome oxidase (CO) (*21*–*23*). The ocular dominance columns are revealed by this approach because metabolic activity is reduced in the missing eye's columns. After perfusion, striate cortex was stripped from the white matter, flattened in a single piece, and sectioned tangentially to the surface. Flatmount preparations enhance the likelihood of detecting subtle metabolic patterns, such as the optic disc representation, which lies buried in the calcarine sulcus (*24*).

Beckman Vision Center, University of California, San Francisco, San Francisco, CA 94143–0730, USA.

*To whom correspondence should be addressed at Beckman Vision Center, University of California, San Francisco, 10 Kirkham Street, San Francisco, CA 94143–0730, USA. E-mail: dadams@itsa.ucsf.edu